

International Journal of Modern Physics B
 © World Scientific Publishing Company

Interplay between quantum phase transitions and the behavior of quantum correlations at finite temperatures

T. Werlang, G. A. P. Ribeiro, and Gustavo Rigolin*

Departamento de Física, Universidade Federal de São Carlos, São Carlos, SP 13565-905, Brazil

Received Day Month Year

Revised Day Month Year

We review the main results and ideas showing that quantum correlations at finite temperatures (T), in particular quantum discord, are useful tools in characterizing quantum phase transitions that only occur, in principle, at the unattainable absolute zero temperature. We first review some interesting results about the behavior of thermal quantum discord for small spin-1/2 chains and show that they already give us important hints of the infinite chain behavior. We then study in detail and in the thermodynamic limit (infinite chains) the thermal quantum correlations for the XXZ and XY models, where one can clearly appreciate that the behavior of thermal quantum discord at finite T is a useful tool to spotlight the critical point of a quantum phase transition.

Keywords: Quantum correlations; Quantum phase transitions; Thermal quantum discord

1. Introduction

A deeper understanding of the low temperature macroscopic phases of a many-body system can only be achieved with the aid of a quantum theory. Of particular interest is the modeling and description of how the system goes from one phase to another, a process known as “phase transition”. In ordinary phase transitions, which occur at finite temperatures, the phase change is driven by thermal fluctuations. For example, if we heat a magnet we arrive at a temperature (Curie temperature) above which it loses its magnetism. In other words, the magnet initially in the ferromagnetic phase, where all spins are aligned, changes to the paramagnetic phase, where the magnetic moments are in a disordered state.

However, a phase transition can also occur at or near absolute zero temperature ($T = 0$), where thermal fluctuations are negligible. This process is called a quantum phase transition (QPT)¹ and is attained varying a tuning parameter in the Hamiltonian (e.g. an external magnetic field) while keeping the temperature fixed. When the tuning parameter reaches a particular value, the so called critical point (CP), the system’s Hamiltonian ground state changes drastically, which reflects in an abrupt modification of the macroscopic properties of the system. In this

*rigolin@ufscar.br

scenario, quantum fluctuations, which loosely speaking are governed by the Heisenberg uncertainty principle, are responsible for the phase transition. Although it is impossible to achieve $T = 0$ due to the third law of thermodynamics, the effects of QPTs can be observed at finite temperatures whenever the de Broglie wavelength is greater than the correlation length of thermal fluctuations¹. Important examples of QPTs are the paramagnetic-ferromagnetic transition in some metals², the superconductor-insulator transition³, and superfluid-Mott insulator transition⁴.

The ground state of a many-body system at $T = 0$ near a CP is often described by a non-trivial wave function due to the long-range correlations among the system's constituents. In Ref. 5 Preskill argued that quantum entanglement could be responsible for these correlations and therefore the methods developed by quantum information theory (QIT) could be useful in studying the critical behavior of many-body systems. Besides, new protocols for quantum computation and communication could be formulated based on such systems. Along these lines many theoretical tools (in particular entanglement quantifiers) originally developed to tackle QIT problems were employed to determine the CPs of QPTs at $T = 0$ ⁶. Later L.-A. Wu et al.⁷ proved a general connection between non-analyticities in bipartite entanglement measures and QPTs while in Ref. 8 this connection was extended to multipartite entanglement.

Recently another quantity, namely, quantum discord (QD), has attracted the attention of the quantum information community. QD goes beyond the concept of entanglement and captures in a certain sense the “quantumness” of the correlations between two parts of a system. It was built by noting the fact that two classically equivalent versions of the mutual information are inequivalent in the quantum domain^{9,10}. Using QD one can show that quantum entanglement does not describe all quantum correlations existing in a correlated quantum state. In other words, it is possible to create quantum correlations other than entanglement between two quantum systems via local operations and classical communication (LOCC).

The first study showing a possible connection between QD and QPT was done by R. Dillenschneider¹¹ in the context of spin chains at $T = 0$, where a CP associated to a QPT was well characterized by QD. Further studies subsequently have confirmed the usefulness of QD in describing other types of QPTs at zero temperature¹². Moreover, it is important to note that such quantum informational approaches to spotlight CPs of QPTs do not require the knowledge of an order parameter (a macroscopic quantity that changes abruptly during the QPT); only the extremal values or the behavior of the derivatives of either the entanglement or QD is sufficient.

The previous theoretical studies, however, were restricted to the zero temperature regime, which is experimentally unattainable; the third law of thermodynamics dictates that it is impossible to drive a system to $T = 0$ by a finite amount of thermodynamic operations. Due to this limitation it is therefore not straightforward to directly compare those theoretical results with experimental data obtained at finite T . In order to overcome this problem one has to study the behavior of quan-

tum correlations in a system at thermal equilibrium, which is described by the canonical ensemble $\rho_T = e^{-H/kT}/Z$, with H being the system's Hamiltonian, k the Boltzmann's constant and $Z = \text{Tr}(e^{-H/kT})$ the partition function. *Thermal entanglement*, i.e. the entanglement computed for states described by ρ_T , was first studied by M. C. Arnesen *et al.*¹³ for a finite unidimensional Heisenberg chain. Other interesting works followed this one, where thermal entanglement has been considered for other Hamiltonians, both for finite^{14,15} and infinite chains¹⁶. See Ref. 17 for extensive reviews on entanglement and QPT. However, the focus of the aforementioned works was not the study of the ability of thermal entanglement to point out CPs when $T > 0$. In Ref. 18, two of us introduced the analogous to thermal entanglement, namely, *thermal quantum discord* (TQD), and we studied the behavior of this quantity in a system consisting of two spins described by the XYZ model in the presence of an external magnetic field. In this work it was observed for the first time that TQD could be able to signal a QPT at *finite* T .

In order to fully explore the previous possibility, highlighted by solving a simple two-body problem¹⁸, we tackled the XXZ Hamiltonian in the thermodynamic limit for several values of $T > 0$ ¹⁹. Now, working with infinite chains, we were able to show for the first time that TQD keeps its ability to detect the CPs associated to the QPTs for the XXZ model even if $T \neq 0$, while entanglement and other thermodynamic quantities are not as good as TQD. Also, we showed that these quantities when contrasted to TQD lose for increasing T their CP-detection property faster than TQD. Later²⁰ we generalized those results considering (i) the XXZ Hamiltonian and (ii) the XY Hamiltonian both in the presence of an external magnetic field. For these two models it was shown that among the usual quantities employed to detect CPs, TQD was the best suited to properly estimate them when $T > 0$.

Our goal in this paper is to present a short but self-contained review of our aforementioned results about TQD and its application as a CP detector of QPTs. To this end we structure this paper as follows. In Sec. 2 we present a brief review about quantum correlations where QD and the entanglement of formation take on a prominent role. In Sec. 3 we review the behavior of TQD in the context of simple two-qubit models. We then move on to the analysis of the ability of quantum correlations, in particular TQD, to spotlight the CPs of QPTs when the system is at $T > 0$ and in the thermodynamic limit. In this context we study the XXZ and XY models with and without an external magnetic field. Finally, we conclude and discuss future directions in Sec. 4.

2. Quantum Correlations

The superposition principle of quantum mechanics is directly related to the existence of (quantum) correlations that are not seen in classical objects. This principle together with the tensorial nature of combining different quantum systems (Hilbert spaces) lead to entanglement, which implies intriguing correlations among the many constituents of a composite system that puzzle our classical minds. It

is worth mentioning that this tensorial nature from which a composite quantum system is described in terms of its parts is not a truism. Indeed, the principle of superposition is also present in classical physics, for example in the classical theory of electromagnetism. However, in classical physics this tensorial nature for combining systems is missing, which helps in understanding why “weird” quantum effects such as non-locality²¹ are not seen in a classical world.

During many decades after the birth of quantum mechanics quantum correlations were thought to be necessarily linked to non-locality, or more quantitatively, to the violation of a Bell-like inequality²². The non-violation of a Bell-like inequality implies that the correlations among the parts of a composite system can be described by a local realistic theory. This fact led many to call a state not violating any Bell-like inequality a classical state.

This situation changed by the seminal work of R. F. Werner²³, who showed that there are mixed entangled states that do not violate any Bell-like inequality. Therefore, according to the Bell/non-locality paradigm these states should be considered examples of classical states although possessing entanglement. This state of affairs was unsatisfactory and the notion of classical states was expanded. A classical (non-entangled) state was then defined as any state that can be created only by local operations on the subsystems and classical communication among its many parts (LOCC)^{24,25}. For a bipartite system described by the density operator ρ_{AB} , the states created via LOCC (separable states) can be generally written as

$$\rho_{AB} = \sum_j p_j \rho_j^A \otimes \rho_j^B, \quad (1)$$

where $p_j \geq 0$, $\sum_j p_j = 1$, and $\rho_j^{A,B}$ are legitimate density matrices. If a quantum state cannot be written as (1) then it is an entangled state.

At this point one may wonder if this is a definitive characterization of a classical state. Or one may ask: Isn't there any “quantumness” in the correlations for some sort of separable (non-entangled) quantum states? Can we go beyond the entanglement paradigm? As observed in refs. 9, 10 there exist some states written as (1) that possess non-classical features. This fact led the authors of refs. 9, 10, 26 to push further our definition of classical states. Now, instead of eq. (1), we call a bipartite state classical if it can be written as

$$\rho_{AB} = \sum_{jk} p_{jk} |j\rangle_A \langle j| \otimes |k\rangle_B \langle k|, \quad (2)$$

where $|j\rangle_A$ and $|k\rangle_B$ span two sets of orthonormal states. States described by (2) are a subset of those described by (1) and they are built via mixtures of locally distinguishable states²⁶. Intuitively, classical states are those where the superposition principle does not manifest itself either on the level of different Hilbert spaces (zero entanglement) or on the level of single Hilbert spaces (no Schrödinger cat states leading to a mixture of non-orthogonal states). Such states have null QD.

Let us be more quantitative and define QD for a bipartite quantum state^{9,10} divided into parts A and B . In the paradigm of classical information theory²⁴ the

total correlation between A and B is quantified by the mutual information (MI),

$$\mathcal{I}_1(A : B) = \mathcal{H}(A) + \mathcal{H}(B) - \mathcal{H}(A, B), \quad (3)$$

where $\mathcal{H}(X) = -\sum_x p_x \log_2 p_x$ is the Shannon entropy with p_x the probability distribution of the random variable X . The conditional probability for classical variables $p_{a|b}$ is defined by the Bayes' rule, that is, $p_{a|b} = p_{a,b}/p_b$, with $p_{a,b}$ denoting the joint probability distribution of variables a and b . Using the conditional probability one can show that $\mathcal{H}(A, B) = \mathcal{H}(A|B) + \mathcal{H}(B)$, where $\mathcal{H}(A|B) = -\sum_{a,b} p_{a,b} \log_2(p_{a|b})$. This last result allows one to write MI, eq. (3), as

$$\mathcal{I}_2(A : B) = \mathcal{H}(A) - \mathcal{H}(A|B). \quad (4)$$

Note that $\mathcal{H}(A|B) \geq 0$ is the conditional entropy, which quantifies how much uncertainty is left on average about A when one knows B . The quantum version of eq. (3), denoted by $\mathcal{I}_1^q(A : B)$, can be obtained replacing the Shannon entropy by the von-Neumann entropy $\mathcal{S}(X) = \mathcal{S}(\rho_X) = -\text{Tr}(\rho_X \log_2 \rho_X)$, where ρ_X is the density operator of the system $X = A, B$. On the other hand, a quantum version of eq. (4) is not so straightforward because the Bayes' rule is not always valid for quantum systems²⁷. For instance, this rule is violated for a pure entangled state. Indeed, one can show that if we naively extend the usual quantum conditional entropy to quantum systems as $\mathcal{S}(A|B) \equiv \mathcal{S}(A, B) - \mathcal{S}(B)$, it becomes negative for pure entangled states. QD is built in a way to circumvent this limitation.

In order to build a meaningful quantum version of the conditional entropy $\mathcal{H}(A|B)$ it is necessary to take into account the fact that knowledge about system B is related to measurements on B . And now, differently from the classical case, a measurement in the quantum domain can be performed in many non-equivalent ways (different set of projectors, for instance). If a general quantum measurement, i.e. a POVM (positive operator valued measure)²⁴, $\{M_b\}$ is performed in the quantum state ρ_{AB} , then after the measurement the state is described by $\sum_b M_b \rho_{AB} M_b^\dagger$. The probability of the outcome b of B is $p_b = \text{Tr}[M_b \rho_{AB} M_b^\dagger]$ and the conditional state of A in this case is $\rho_{A|b} = (M_b \rho_{AB} M_b^\dagger) / p_b$. Thus, the conditional entropy with respect to the POVM $\{M_b\}$ is $\mathcal{S}(A|\{M_b\}) \equiv \sum_b p_b \mathcal{S}(\rho_{A|b})$. Therefore, in order to quantify the uncertainty left on A after a measurement on B one has to minimize over all POVMs. This leads to the following definition of the quantum conditional entropy^{9,10}:

$$\mathcal{S}_q(A|B) \equiv \min_{\{M_b\}} \mathcal{S}(A|\{M_b\}). \quad (5)$$

At this point, the quantum version of the mutual information (4), denoted by $\mathcal{I}_2^q(A : B)$, is obtained replacing the classical conditional entropy $\mathcal{H}(A|B)$ by its quantum analog $\mathcal{S}_q(A|B)$, which does not assume negative values. The *quantum discord* is defined as the difference between these two versions of the quantum mutual

information^{9,10}:

$$\begin{aligned} D(A|B) &\equiv \mathcal{I}_1^q(A : B) - \mathcal{I}_2^q(A : B) \\ &= \mathcal{S}_q(A|B) - \mathcal{S}(A|B). \end{aligned} \quad (6)$$

Note that QD is not necessarily a symmetric quantity, because the conditional entropy (5) depends on the system in which the measurement is performed. However, for the density operators studied in this paper QD is always symmetric. Furthermore, while for mixed states there are states with null entanglement and $\text{QD} > 0$, for pure states QD is essentially equivalent to entanglement. In other words, only for mixed states there might be quantum correlations other than entanglement. As demonstrated recently²⁸, a quantum state ρ_{AB} has $D(A|B) = 0$ if, and only if, it can be written as $\rho_{AB} = \sum_j p_j \rho_j^A \otimes |\psi_j^B\rangle \langle \psi_j^B|$, with $\sum_j p_j = 1$ and $\{|\psi_j^B\rangle\}$ a set of orthogonal states. This result shows the importance of the superposition principle to explain the origin of the quantum correlations. It is due to this principle that one can generate a set $\{|\psi_j^B\rangle\}$ of non-orthogonal states leading to states with nonzero QD.

For arbitrary $N \times M$ -dimensional bipartite states the computation of QD involves a complicated minimization procedure whose origin can be traced back to the evaluation of the conditional entropy $\mathcal{S}_q(A|B)$, eq. (5). In general one must then rely on numerical procedures to get QD and it is not even known whether a general efficient algorithm exists. For two-qubit systems, however, the minimization over generalized measurements can be replaced by the minimization over projective measurements (von Neumann measurements)²⁹. In this case the minimization procedure can be efficiently implemented numerically³⁰ for arbitrary two-qubit states and some analytical results can be achieved for a restricted class of states³¹. In this work we will be dealing with density matrices ρ in the X-form, that is, $\rho_{12} = \rho_{13} = \rho_{24} = \rho_{34} = 0$. Moreover, in our models $\rho_{22} = \rho_{33}$ and all matrix elements are real, making the numerical evaluation of QD simple and fast.

To close this section, we introduce the measure of entanglement used in this paper, the *Entanglement of Formation* (EoF)³². EoF quantifies, at least for pure states, how many singlets are needed per copy of ρ_{AB} to prepare many copies of ρ_{AB} using only LOCC. For an X-form density matrix we have

$$\text{EoF}(\rho_{AB}) = -g \log_2 g - (1 - g) \log_2 (1 - g), \quad (7)$$

with $g = (1 + \sqrt{1 - C^2})/2$ and the concurrence³² given by $C = 2 \max\{0, \Lambda_1, \Lambda_2\}$, where $\Lambda_1 = |\rho_{14}| - \sqrt{\rho_{22}\rho_{33}}$ and $\Lambda_2 = |\rho_{23}| - \sqrt{\rho_{11}\rho_{44}}$.

3. Results and Discussions

3.1. Two interacting spins

In this section we consider a two spin system described by the XYZ model with an external magnetic field acting on both spins.¹⁸ The Hamiltonian of this model is

$$H_{XYZ} = \frac{J_x}{4} \sigma_1^x \sigma_2^x + \frac{J_y}{4} \sigma_1^y \sigma_2^y + \frac{J_z}{4} \sigma_1^z \sigma_2^z + \frac{B}{2} (\sigma_1^z + \sigma_2^z), \quad (8)$$

where σ_j^α ($\alpha = x, y, z$) are the usual Pauli matrices acting on the j -th site and we have assumed $\hbar = 1$. As mentioned above, the density matrix describing a system in equilibrium with a thermal reservoir at temperature T is $\rho_T = e^{-H/kT}/Z$, where $Z = \text{Tr}(e^{-H/kT})$ is the partition function. Therefore, the thermal state for the Hamiltonian (8) assumes the following form

$$\rho = \frac{1}{Z} \begin{pmatrix} A_{11} & 0 & 0 & A_{12} \\ 0 & B_{11} & B_{12} & 0 \\ 0 & B_{12} & B_{11} & 0 \\ A_{12} & 0 & 0 & A_{22} \end{pmatrix}, \quad (9)$$

with $A_{11} = e^{-\alpha} (\cosh(\beta) - 4B \sinh(\beta)/\eta)$, $A_{12} = -\Delta e^{-\alpha} \sinh(\beta)/\eta$, $A_{22} = e^{-\alpha} (\cosh(\beta) + 4B \sinh(\beta)/\eta)$, $B_{11} = e^\alpha \cosh(\gamma)$, $B_{12} = -e^\alpha \sinh(\gamma)$, and $Z = 2(\exp(-\alpha) \cosh(\beta) + \exp(\alpha) \cosh(\gamma))$, where $\Delta = J_x - J_y$, $\Sigma = J_x + J_y$, $\eta = \sqrt{\Delta^2 + 16B^2}$, $\alpha = J_z/(4kT)$, $\beta = \eta/(4kT)$, and $\gamma = \Sigma/(4kT)$.

The first important result appears in the absence of an external field. As shown in Ref. 15, when $B = 0$, the entanglement does not increase with increasing temperature. On the other hand, as can be seen in Fig. 1 (panels *a* and *b*) for the XXZ model ($J_x = J_y = J$ and $J_z \neq 0$), TQD begins with a non-null value at $T = 0$ and increases as T increases before decreasing with T , while EoF is always zero¹⁵. Note that such effect is observed for different configurations of coupling constants.

The possibility of TQD to point out a QPT even when the system is at finite temperatures emerged from our study about the XXX model for two spins¹⁸. The XXX model is obtained from Hamiltonian (8) making $J_x = J_y = J_z = J$. When $J \rightarrow \infty$ the density operator (9) will be the Bell state $\rho = |\psi\rangle\langle\psi|$, with $|\psi\rangle = \frac{1}{\sqrt{2}}(|01\rangle - |10\rangle)$, for any T . For the opposite limit $J \rightarrow -\infty$ the density operator is the mixed state $\rho = \frac{1}{3}(|00\rangle\langle 00| + |11\rangle\langle 11| + |\phi\rangle\langle\phi|)$ with $|\phi\rangle = \frac{1}{\sqrt{2}}(|01\rangle + |10\rangle)$. In this case EoF is zero, while TQD assumes the value 1/3. Furthermore, as shown in Fig. 2, EoF is zero in the ferromagnetic region ($J < 0$) and non-zero in the antiferromagnetic region ($J > 0$) only when $T = 0$. For $T > 0$ EoF becomes non-zero only for $J > J_c(T) = kT \ln(3)$. On the other hand, TQD is equal to zero only at the trivial point $J = 0$, even at finite T . Although we are considering here only two spins, such result suggests that TQD may possibly signal a QPT for $T > 0$.

Let us now analyze the case where $B \neq 0$ and focus on the XY model in a transverse magnetic field ($J_x, J_y \neq 0$, and $J_z = 0$). As noted in Ref. 15 EoF shows a sudden death and then a revival (see Fig. 3, panel *b*). However, TQD does not suddenly disappear as Fig. 3, panel *a*, depicts. Actually, TQD decreases with T

8 Authors' Names

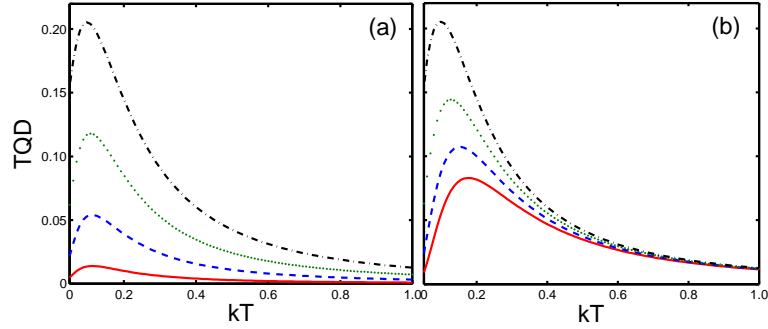


Fig. 1. TQD for a two spin system as a function of the absolute temperature kT for the XXZ model with $B = 0$. (a) Here $J_z = -0.5$ and $J = 0.1$ (solid line), 0.2 (dashed line), 0.3 (dotted line), 0.4 (dash-dotted line); (b) Now we fix $J = 0.4$ and $J_z = -0.8$ (solid line), -0.7 (dashed line), -0.6 (dotted line), -0.5 (dash-dotted line). Here and in the following graphics all quantities are dimensionless.

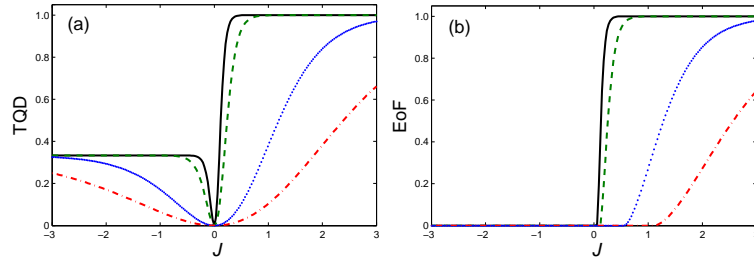


Fig. 2. TQD (a) and EoF (b) for a two spin system as functions of the coupling J for $kT = 0.05$ (solid line), 0.1 (dashed line), 0.5 (dotted line), 1.0 (dash-dotted line). Both plots for the XXX model with $B = 0$.

to a non-null value and after a critical temperature T_c it starts increasing again. This effect is called *regrowth*¹⁸. Although the regrowth of EoF with temperature is not observed for two spin chains, we showed in Ref. 20 that such interesting behavior is possible in the thermodynamic limit. Also, if we carefully look at Fig. 3 the distinctive aspects of these two types of quantum correlations become more evident. For example, comparing panels a and b we see regions where TQD increases while EoF decreases. Finally, in a very interesting and recent work, X. Rong *et al.*³³ experimentally verified some of the predictions here revised and reported in refs. 18, 19, 20, namely, the sudden change of TQD at finite temperatures while changing the anisotropy parameter of a two spin XXZ Hamiltonian.

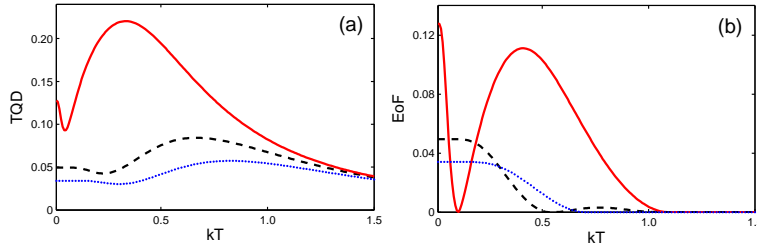


Fig. 3. TQD (a) and EoF (b) for a two spin system as functions of the absolute temperature kT for the XY model with transverse magnetic field B . Here $J_x = 2.6$ and $J_y = 1.4$. The values for B are 1.1 (solid line), 2.0 (dashed line), and 2.5 (dotted line).

3.2. XXZ Model

Turning our attention to infinite chains ($L \rightarrow \infty$), let us start working with the one-dimensional anisotropic spin-1/2 XXZ model subjected to a magnetic field in the z -direction. Its Hamiltonian is

$$H_{xxz} = J \sum_{j=1}^L (\sigma_j^x \sigma_{j+1}^x + \sigma_j^y \sigma_{j+1}^y + \Delta \sigma_j^z \sigma_{j+1}^z) - \frac{h}{2} \sum_{j=1}^L \sigma_j^z, \quad (10)$$

where Δ is the anisotropy parameter, h is the external magnetic field, and J is the exchange constant ($J = 1$). We have assumed periodic boundary conditions ($\sigma_{L+1}^\alpha = \sigma_1^\alpha$). The nearest neighbor two spin state is obtained by tracing all but the first two spins, $\rho_{1,2} = \text{Tr}_{L-2}(\rho)$, where $\rho = \exp(-\beta H_{xxz})/Z$. The Hamiltonian (10) exhibits both translational invariance and $U(1)$ invariance ($[H_{xxz}, \sum_{j=1}^L \sigma_j^z] = 0$) leading to the following nearest neighbor two spin state

$$\rho_{1,2} = \frac{1}{4} \begin{pmatrix} \rho_{11} & 0 & 0 & 0 \\ 0 & \rho_{22} & \rho_{23} & 0 \\ 0 & \rho_{23} & \rho_{22} & 0 \\ 0 & 0 & 0 & \rho_{44} \end{pmatrix}, \quad (11)$$

where

$$\begin{aligned} \rho_{11} &= 1 + 2 \langle \sigma^z \rangle + \langle \sigma_1^z \sigma_2^z \rangle, \\ \rho_{22} &= 1 - \langle \sigma_1^z \sigma_2^z \rangle, \\ \rho_{44} &= 1 - 2 \langle \sigma^z \rangle + \langle \sigma_1^z \sigma_2^z \rangle, \\ \rho_{23} &= 2 \langle \sigma_1^x \sigma_2^x \rangle. \end{aligned} \quad (12)$$

The magnetization and the two-point correlations above are obtained in terms

of the derivatives of the free-energy³⁴, $f = -\frac{1}{\beta} \lim_{L \rightarrow \infty} \frac{\ln Z}{L}$,

$$\begin{aligned}\langle \sigma^z \rangle &= -2\partial_h f / J, \\ \langle \sigma_j^z \sigma_{j+1}^z \rangle &= \partial_\Delta f / J, \\ \langle \sigma_j^x \sigma_{j+1}^x \rangle &= \frac{u - \Delta \partial_\Delta f + h \langle \sigma^z \rangle}{2J}, \\ \langle \sigma_j^z \sigma_{j+1}^z \rangle &= \langle \sigma_j^x \sigma_{j+1}^x \rangle = \frac{u + h \langle \sigma^z \rangle}{3J}, \quad \Delta = 1,\end{aligned}$$

where $u = \partial_\beta(\beta f)$ is the internal energy. We explained in details the procedures to determine the free-energy f in Ref. 20. It is not a simple task and it involves the application of complicated analytical and numerical computations. The CPs of the XXZ model depend on the value of the magnetic field h ³⁵. One of them, called Δ_{inf} , is an infinite-order QPT determined by solving the following equation,

$$h = 4J \sinh(\eta) \sum_{n=-\infty}^{\infty} \frac{(-1)^n}{\cosh(n\eta)}, \quad (13)$$

with $\eta = \cosh^{-1}(\Delta_{inf})$. The other CP, called Δ_1 , is a first-order QPT given by

$$\Delta_1 = \frac{h}{4J} - 1. \quad (14)$$

The behavior of TQD and EoF for the XXZ model at finite T and $h = 0$ was initially studied in ref. 19. For $h = 0$ the XXZ model has two CPs³⁶. At $\Delta_{inf} = 1$ the ground state changes from an XY-like phase ($-1 < \Delta < 1$) to an Ising-like antiferromagnetic phase ($\Delta > 1$). At $\Delta_1 = -1$ it changes from a ferromagnetic phase ($\Delta < -1$) to the critical antiferromagnetic phase ($-1 < \Delta < 1$). In ref. 19 we analyzed the behavior of TQD and EoF only for $\Delta > 0$. Here we extend those results by computing the correlation functions for the remaining values of the anisotropy parameter, namely, $\Delta < 0$. In Fig. 4 we plot TQD (panel a) and EoF (panel c) as a function of Δ for different values of kT and $h = 0$. For $T = 0$ we can see that both TQD and EoF are able to detect the CPs. TQD is discontinuous at Δ_1 while at Δ_{inf} the first-order derivative of TQD presents a discontinuity. Furthermore, EoF is zero for $\Delta < \Delta_1$ and non-zero for $\Delta > \Delta_1$ reaching a maximum value at $\Delta = \Delta_{inf}$. However, as the temperature increases the maximum value of EoF is shifted to the right. Besides, EoF becomes zero also for $\Delta > \Delta_1$ as we increase T . On the other hand, the first-order derivative of TQD is still discontinuous at $\Delta_{inf} = 1$ for finite T . We can also observe that TQD increases for $\Delta < -1$ as T increases while its first-order derivative diverges at the CP $\Delta = -1$. As mentioned in Ref. 19 the cusp-like behavior at CPs $\Delta_1 = 1$ and $\Delta_{inf} = -1$ is due to an exchange in the set of projectors that minimizes the quantum conditional entropy (5).

The study about the XXZ model was further explored in Ref. 20, with the addition of an external field. The effects of the magnetic field h on the quantum correlations are exemplified in Fig. 4 (panels b and d), where we set $h = 12$. The values of the CPs for $h = 12$ are calculated employing Eqs. (13) and (14), resulting

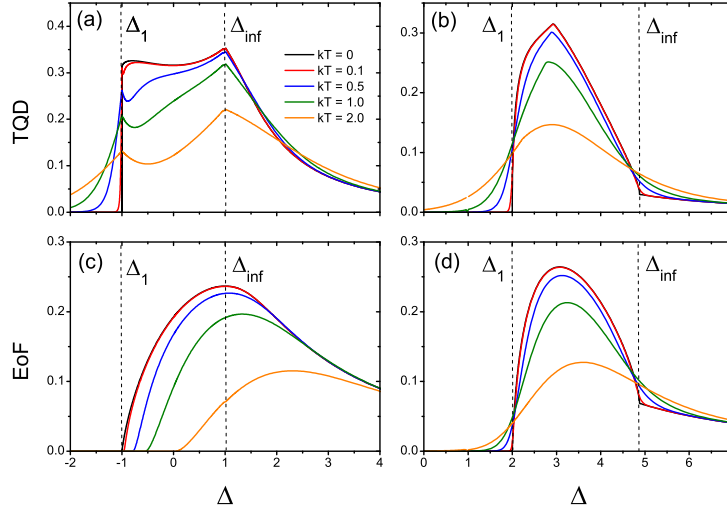


Fig. 4. TQD (panels a and b) and EoF (panels c and d) as functions of the tuning parameter Δ for $h = 0$ (panels a and c) and $h = 12$ (panels b and d). From top to bottom in the region where $\Delta_1 < \Delta < \Delta_{inf}$, $kT = 0, 0.1, 0.5, 1.0, 2.0$.

in $\Delta_{inf} \approx 4.88$ and $\Delta_1 = 2$. Again, for $T = 0$ the CPs are detected by both TQD and EoF and, differently from the case $h = 0$, the behavior of these two quantities is quite similar. Both quantities are zero for $\Delta < 2$ and non-zero for $\Delta > 2$, with their first-order derivatives diverging at the CP $\Delta_1 = 2$. However, the infinite-order QPT is no longer characterized by a global maximum of TQD or EoF, but by a discontinuity in their first-order derivatives. Note also that TQD presents a cusp-like behavior between the CPs. This behavior is once again related to the minimization procedure of the quantum conditional entropy and so far it is not associated to any known QPT for this model. It is important to mention that entanglement measures may also have a discontinuity and/or a divergence in their derivatives that are not related to a QPT³⁷.

Now we move on to the cases where $T > 0$. When T increases both curves of TQD and EoF become smoother and broader, with well defined derivatives in the CPs. Besides, the cusp-like behavior of TQD previously mentioned tends to disappear while both maximums of TQD and EoF decrease²⁰. We noted in Ref. 20 that some features of the derivatives of these quantities remain for a finite, but not too high temperature. To illustrate this fact, we plotted in Fig. 5 the first-order (panel a) and second-order (panel b) derivatives of TQD with respect to the anisotropy parameter Δ for $h = 12$ and $kT = 0.02, 0.1, 0.5$. To plot the curves for different temperatures in the same graph we normalized the derivatives of TQD, that is, for each T we plotted the derivative of TQD divided by the maximum value of the respective derivative. For $T = 0$ the divergence in the first-order derivative of both TQD and EoF spotlights the CP Δ_1 while the CP Δ_{inf} is characterized

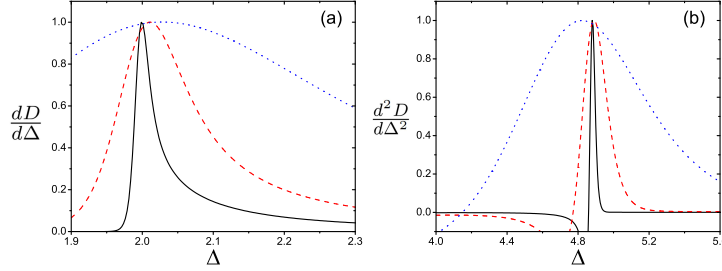


Fig. 5. First-order (panel a) and second-order (panel b) derivatives of TQD as functions of Δ for the XXZ model with $h = 12$ and for $kT = 0.02$ (solid line), $kT = 0.1$ (dashed line), and $kT = 0.5$ (dotted line). The derivatives plotted here are normalized, that is, each curve was divided by the maximum value of the respective derivative. The maximum of the first-order and second-order derivatives of TQD are very close to the CPs $\Delta_1 = 2$ and $\Delta_{inf} \approx 4.88$, respectively.

by a divergence in the second-order derivative. As can be seen in Fig. 5, although the divergence at the CPs disappears as T increases, the derivatives reach their maximum values around the CPs. We used these maximum values to estimate the CPs at finite temperatures. The same analysis was applied to estimate the CPs using EoF instead of TQD. In Ref. 20 we compared the ability of TQD, EoF, and pairwise correlations ($\langle \sigma_1^z \sigma_2^z \rangle$ and $\langle \sigma_1^x \sigma_2^x \rangle$) to point out the CPs for $T > 0$ and we showed that TQD is the best candidate to estimate the CPs.

To illustrate such result we compared in Fig. 6 the difference between the correct CP Δ_c and the CP estimated by our method Δ_e for $h = 6$ and $h = 12$. One can see in this figure that from zero to $kT \approx 1$ the CPs estimated by TQD are closer to the correct ones than the estimated CPs coming from other quantities.

3.3. XY Model

The Hamiltonian of the one-dimensional XY model in a transverse field is given by

$$H_{xy} = -\frac{\lambda}{2} \sum_{j=1}^L [(1 + \gamma)\sigma_j^x \sigma_{j+1}^x + (1 - \gamma)\sigma_j^y \sigma_{j+1}^y] - \sum_{j=1}^L \sigma_j^z, \quad (15)$$

where λ is the strength of the inverse of the external transverse magnetic field and γ is the anisotropy parameter. The transverse Ising model is obtained for $\gamma = \pm 1$ while $\gamma = 0$ corresponds to the XX model in a transverse field³⁸. At $\lambda_c = 1$ the XY model undergoes a second-order QPT (Ising transition³⁹) that separates a ferromagnetic ordered phase from a quantum paramagnetic phase. Another second order QPT is observed for $\lambda > 1$ at the CP $\gamma_c = 0$ (anisotropy transition^{38,40}). This transition is driven by the anisotropy parameter γ and separates a ferromagnet ordered along the x direction and a ferromagnet ordered along the y direction. These two transitions are of the same order but belong to different universality classes^{38,40}.

The XY Hamiltonian is Z_2 -symmetric and can be exactly diagonalized³⁸ in the

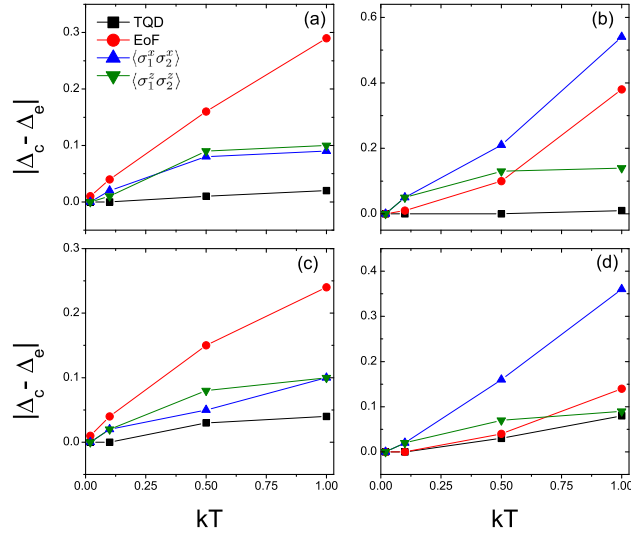


Fig. 6. The difference between the correct CP and the CP estimated by TQD (square), EoF (circle), $\langle \sigma_1^x \sigma_2^x \rangle$ (up arrow), and $\langle \sigma_1^z \sigma_2^z \rangle$ (down arrow) as a function of kT . In (a) and (b) we have $h = 6$ with a first (a) and an infinite-order (b) CP; in (c) and (d) we have $h = 12$ with a first (c) and an infinite-order (d) CP. Δ_c denotes the correct value of CP while Δ_e denotes the value of CP estimated by the extremum values of the derivatives of the quantities involved.

thermodynamic limit $L \rightarrow \infty$. Due to translational invariance the two spin density operator $\rho_{i,j}$ for spins i and j at thermal equilibrium is⁴¹

$$\rho_{0,k} = \frac{1}{4} [I_{0,k} + \langle \sigma^z \rangle (\sigma_0^z + \sigma_k^z)] + \frac{1}{4} \sum_{\alpha=x,y,z} \langle \sigma_0^\alpha \sigma_k^\alpha \rangle \sigma_0^\alpha \sigma_k^\alpha, \quad (16)$$

where $k = |j - i|$ and $I_{0,k}$ is the identity operator of dimension four. The transverse magnetization $\langle \sigma_k^z \rangle = \langle \sigma^z \rangle$ is

$$\langle \sigma^z \rangle = - \int_0^\pi (1 + \lambda \cos \phi) \tanh(\beta \omega_\phi) \frac{d\phi}{2\pi \omega_\phi}, \quad (17)$$

with $\omega_\phi = \sqrt{(\gamma \lambda \sin \phi)^2 + (1 + \lambda \cos \phi)^2}/2$. The two-point correlation functions are

given by

$$\langle \sigma_0^x \sigma_k^x \rangle = \begin{vmatrix} G_{-1} & G_{-2} & \cdots & G_{-k} \\ G_0 & G_{-1} & \cdots & G_{-k+1} \\ \vdots & \vdots & \ddots & \vdots \\ G_{k-2} & G_{k-3} & \cdots & G_{-1} \end{vmatrix}, \quad (18)$$

$$\langle \sigma_0^y \sigma_k^y \rangle = \begin{vmatrix} G_1 & G_0 & \cdots & G_{-k+2} \\ G_2 & G_1 & \cdots & G_{-k+3} \\ \vdots & \vdots & \ddots & \vdots \\ G_k & G_{k-1} & \cdots & G_1 \end{vmatrix}, \quad (19)$$

$$\langle \sigma_0^z \sigma_k^z \rangle = \langle \sigma^z \rangle^2 - G_k G_{-k}, \quad (20)$$

where

$$G_k = \int_0^\pi \tanh(\beta\omega_\phi) \cos(k\phi) (1 + \lambda \cos \phi) \frac{d\phi}{2\pi\omega_\phi} \\ - \gamma\lambda \int_0^\pi \tanh(\beta\omega_\phi) \sin(k\phi) \sin \phi \frac{d\phi}{2\pi\omega_\phi}.$$

The relation between TQD and QPT for the Ising model (XY model with $\gamma = 1$) at $T = 0$ was investigated initially by Dillenschneider¹¹ for first and second nearest-neighbors. More general results were obtained in Ref. 42 where TQD and EoF from first to fourth nearest-neighbors was computed for different values of γ . This study at $T = 0$ showed that while EoF between far neighbors becomes zero, QD is not null and detects the QPT. The effects of the symmetry breaking process in entanglement and QD for the XY and the XXZ models were discussed in Refs. 43, where the low temperature regime was taken into account. In Ref. 20 we compared the ability of TQD and EoF for first and second nearest-neighbors to detect the CPs for the XY model at finite temperature.

The behavior of TQD and EoF for first nearest-neighbors as a function of λ for $kT = 0.01, 0.1, 0.5$ and $\gamma = 0, 0.5, 1.0$ can be seen in Fig. 7. First, note that TQD is more robust to temperature increase than EoF. For $kT = 0.5$ TQD is always non-zero while EoF is zero or close to zero for almost all λ (see the blue/solid curves in Fig. 7). As showed in Ref. 20, for second nearest-neighbors the situation is more drastic since EoF is always zero for $kT = 0.5$. Now, to estimate the CPs at finite T we used the same procedure adopted for the XXZ model. If the first-order derivative of TQD or EoF is divergent at $T = 0$ then the CP is pointed out by a local maximum or minimum at $T > 0$; if the first-order derivative is discontinuous at $T = 0$ then we look after local maximum or minimum in the second derivative for $T > 0$. These extreme values act as indicators of QPTs. The CPs estimated with such method are denoted by λ_e while the correct CPs are denoted by λ_c . The differences between λ_c and λ_e as a function of kT for $\gamma = 0, 0.5, 1.0$ are plotted in Fig. 8. We can see in this figure that TQD provides a better estimate of the CP $\lambda_c = 1$ than EoF.

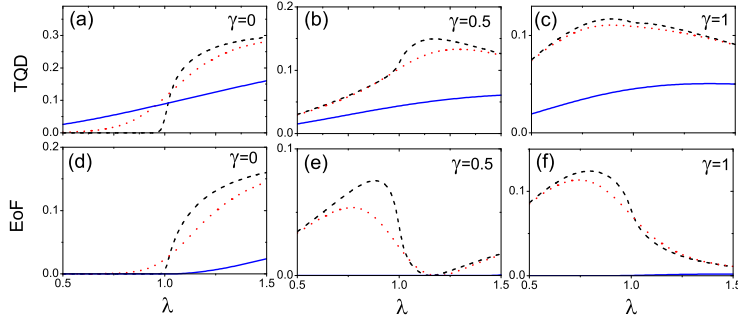


Fig. 7. (a)-(c) TQD and (d)-(f) EoF as functions of λ for $kT = 0.01$ (black/dashed line), $kT = 0.1$ (red/dotted line) and $kT = 0.5$ (blue/solid line) for nearest-neighbors. We use three values of γ as shown in the graphs.

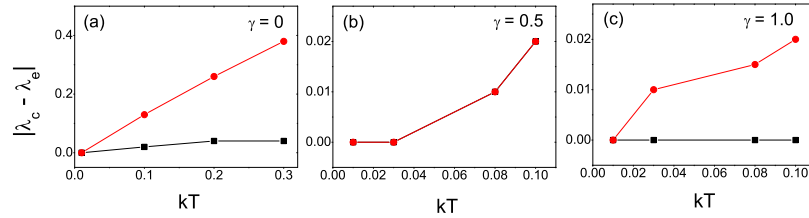


Fig. 8. The difference between the correct CP, λ_c , and, λ_e , the CP estimated either by TQD (square) or EoF (circle) as a function of kT for (a) $\gamma = 0$, (b) $\gamma = 0.5$, and (c) $\gamma = 1.0$. Note that both curves coincide at panel (b).

For $\gamma = 0.5$ EoF and TQD give almost the same estimation of the CP and for $\gamma = 1.0$ TQD is better than EoF with predictions differing at the second decimal place. For $\gamma = 0$, TQD outperforms EoF already in the first decimal place. Moreover, for $\gamma = 0$ TQD is able to correctly estimate the CP for higher temperatures than for $\gamma = 0.5$ and $\gamma = 1.0$.

So far we have studied a QPT driven by the magnetic field. However, for $\lambda > 1$ the XY model undergoes a QPT driven by the anisotropy parameter γ , whose critical point is $\gamma_c = 0$. To study such transition we fixed $\lambda = 1.5$. In Fig. 9 we plotted TQD and EoF for the first-neighbors as functions of γ and for $kT = 0.001, 0.1, 0.5, 1.0$, and 2.0 . Note that the maximum of TQD and EoF is reached at the CP $\gamma_c = 0$. However, only TQD has a cusp-like behavior at the CP. This pattern of TQD (maximum with a cusp-like behavior) remains up to $kT = 2.0$. On the other hand, the maximum of EoF at the CP can only be seen as far as $kT < 1$ for above this temperature EoF becomes zero. In Ref. 20 we computed TQD and EoF for second-neighbors. In this case TQD is able to detect the CP even for values near $kT = 1.0$ while EoF is nonzero only for $kT \lesssim 0.1$.

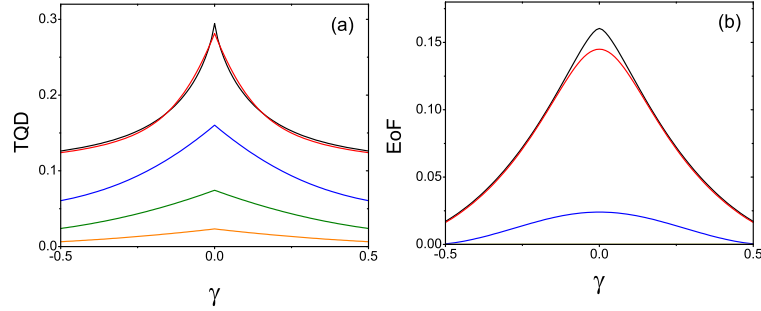


Fig. 9. (a) TQD and (b) EoF for the first nearest-neighbors as functions of γ . From top to bottom $kT = 0.001, 0.1, 0.5, 1.0$, and 2.0 . Here we fixed $\lambda = 1.5$ and the CP is $\gamma_c = 0$.

4. Conclusions

In this article we presented a review of our studies about the behavior of quantum correlations in the context of spin chains at finite temperatures. The main goal of this paper was to analyze the quantum correlation's ability to pinpoint the critical points associated to quantum phase transitions assuming the system's temperature is greater than the absolute zero. The two measures of quantum correlations studied here were quantum discord and entanglement, with the former producing the best results.

We first reviewed a work of two of us about a simple but illustrative two spin-1/2 system described by the XYZ model with an external magnetic field¹⁸. We showed many surprising results about the thermal quantum discord's behavior. For example, and differently from entanglement, thermal quantum discord can increase with temperature in the absence of an external field even for such a small system; and that there are situations where thermal quantum discord increases while entanglement decreases with temperature. Furthermore, for the XXX model we observed for the first time that quantum discord could be a good candidate to signal a critical point at finite T .

To check whether quantum discord is indeed a good critical point detector for temperatures higher than absolute zero, we analyzed its behavior for an infinite chain described by the XXZ model without¹⁹ and with²⁰ an external magnetic field and in equilibrium with a thermal reservoir at temperature T . Here we also extended our previous results by computing the quantum correlations between the first nearest-neighbor spins for the whole range of the anisotropy parameter (positive and negative values). In this way we were able to describe the two critical points of the XXZ model in the thermodynamic limit and the behavior of quantum discord near them. The results presented here and in refs. 19, 20 showed that quantum discord is far better the best critical point detector for $T > 0$ with respect to all quantities tested (entanglement, entropy, specific heat, magnetic susceptibility, and the two-point correlation functions).

Another model considered in this work was the XY model in a transverse magnetic field²⁰. Again, we computed the quantum correlations between the first nearest-neighbors assuming the system in equilibrium with a thermal reservoir at temperature T . This model has two second-order quantum phase transitions, namely, an Ising transition and an anisotropy transition. For the Ising transition we observed that the critical point is better estimated by quantum discord. For the anisotropy transition both quantities, entanglement and discord, provide an excellent estimate for the critical point at low temperatures. However, since for increasing temperatures quantum discord is more robust than entanglement, the former was able to spotlight the quantum critical point for a wider range of temperatures, even for values of temperature where entanglement was absent.

In conclusion, we showed that for the spin models studied here and in Refs. 19, 20 quantum discord was the best quantum critical point estimator among all quantities tested when the system assumes a finite temperature. It is also important to mention that the knowledge of the order parameter was not needed to estimate the critical points. Therefore, we strongly believe that our results suggest that quantum correlations - mainly quantum discord - are important tools to study quantum phase transitions in realistic scenarios, where the temperature is always above absolute zero.

Acknowledgements

TW and GR thank the Brazilian agency CNPq (National Council for Scientific and Technological Development) for funding and GAPR thanks CNPq and FAPESP (State of São Paulo Research Foundation) for funding. GR also thanks CNPq/FAPESP for financial support through the National Institute of Science and Technology for Quantum Information.

1. S. Sachdev, *Quantum Phase Transitions* (Cambridge University Press, Cambridge, 1999).
2. S. Rowley *et al.*, Phys. Status Solid B **247**, 469 (2010).
3. V. F. Gantmakher and V. T. Dolgoplov, Physics-Uspekhi **53**, 1 (2010).
4. M. Greiner *et al.*, Nature (London) **415**, 39 (2002).
5. J. Preskill, J. Mod. Opt. **47**, 127 (2000).
6. T. J. Osborne and M. A. Nielsen, Phys. Rev. A **66**, 032110 (2002); A. Osterloh *et al.*, Nature(London) **416**, 608 (2002); J. I. Latorre, E. Rico, and G. Vidal, Quantum Inf. Comp. **4**, 48 (2004); G. Vidal *et al.*, Phys. Rev. Lett. **90**, 227902 (2003); R. Somma *et al.*, Phys. Rev. A **70**, 042311 (2004); T. -C. Wei *et al.*, Phys. Rev. A **71**, 060305 (2005); F. Verstraete, M. Popp, and J. I. Cirac, Phys. Rev. Lett. **92**, 027901 (2004); M. Popp *et al.*, Phys.Rev. A **71**, 042306 (2005).
7. L.-A. Wu, M. S. Sarandy, and D. A. Lidar, Phys. Rev. Lett. **93**, 250404 (2004).
8. T. R. de Oliveira *et al.*, Phys. Rev. Lett. **97**, 170401 (2006); T. R. de Oliveira, G. Rigolin, and M. C. de Oliveira, Phys. Rev. A **73**, 010305(R) (2006); G. Rigolin, T. R. de Oliveira, and M. C. de Oliveira, Phys. Rev. A **74**, 022314 (2006).
9. H. Ollivier and W. H. Zurek, Phys. Rev. Lett. **88**, 017901 (2001).
10. L. Henderson and V. Vedral, J. Phys. A: Math. Gen. **34**, 6899 (2001).
11. R. Dillenschneider, Phys. Rev. B **78**, 224413 (2008).

12. M. S. Sarandy, Phys. Rev. A **80**, 022108 (2009); C. C. Rulli and M. S. Sarandy, Phys. Rev. A **81**, 032334 (2010); C. C. Rulli and M. S. Sarandy, Phys. Rev. A **84**, 042109 (2011); A. Saguia et al., Phys. Rev. A **84**, 042123 (2011); M. Allegra, P. Giorda, and A. Montorsi, Phys. Rev. B **84**, 245133 (2011).
13. M. C. Arnesen, S. Bose, and V. Vedral, Phys. Rev. Lett. **87**, 017901 (2001).
14. G. L. Kamta and A. F. Starace, Phys. Rev. Lett. **88**, 107901 (2002); X. Wang, Phys. Rev. A **64**, 012313 (2001); Y. Sun, Y. Chen, and H. Chen, Phys. Rev. A **68**, 044301 (2003); S.-J. Gu, H.-Q. Lin, and Y.-Q. Li, Phys. Rev. A **68**, 042330 (2003).
15. G. Rigolin, Int. J. Quant. Inf. **2**, 393 (2004).
16. L. Amico and D. Patané, Europhys. Lett. **77**, 17001 (2007).
17. L. Amico *et al.*, Rev. Mod. Phys. **80**, 517 (2008); L. Amico and R. Fazio, J. Phys. A: Math. Theor. **42**, 504001 (2009).
18. T. Werlang and G. Rigolin, Phys. Rev. A **81**, 044101 (2010).
19. T. Werlang, C. Trippé, G.A.P. Ribeiro and G. Rigolin, Phys. Rev. Lett. **105**, 095702 (2010).
20. T. Werlang, G.A.P. Ribeiro and G. Rigolin, Phys. Rev. A **83**, 062334 (2011).
21. A. Einstein, B. Podolsky, and N. Rosen, Phys. Rev. **47**, 777 (1935).
22. J. S. Bell, Physics **1**, 195 (1964).
23. R. F. Werner, Phys. Rev. A **40**, 4277 (1989).
24. M. A. Nielsen and I. L. Chuang, *Quantum Computation and Quantum Information*. (Cambridge University Press, Cambridge, 2000).
25. R. Horodecki *et al.*, Rev. Mod. Phys. **81**, 865 (2009).
26. K. Modi *et al.*, Phys. Rev. Lett. **104**, 080501 (2010).
27. A. Peres, *Quantum Theory: Concepts and Methods*. (Kluwer Academic Publishers, New York, 2002).
28. B. Dakic, V. Vedral, C. Brukner, Phys. Rev. Lett. **105**, 190502 (2010).
29. S. Hamieh, R. Kobes, and H. Zaraket, Phys. Rev. A **70**, 052325 (2004).
30. D. Girolami and G. Adesso, Phys. Rev. A **83**, 052108 (2011).
31. M. Ali, A. R. P. Rau, and G. Alber, Phys. Rev. A **81**, 042105 (2010); *ibid.* **82**, 069902(E) (2010).
32. W. K. Wootters, Phys. Rev. Lett. **80**, 2245 (1998).
33. X. Rong *et al.*, eprint arXiv:1203.3960v1 [quant-ph].
34. M. Bortz and F. Göhmann, Eur. Phys. J. B **46**, 399 (2005); H.E. Boos *et al.*, J. Stat. Mech. (2008) P08010; C. Trippé, F. Göhmann, and A. Klümper, Eur. Phys. J. B **73**, 253 (2010).
35. J. Cloizeaux and M. Gaudin, J. Math. Phys. **7**, 1384 (1966).
36. M. Takahashi, *Thermodynamics of one-dimensional solvable models* (Cambridge University Press, Cambridge, England, 1999).
37. Min-Fong Yang, Phys. Rev. A **71**, 030302 (2005).
38. E. Lieb, T. Schultz, and D. Mattis, Ann. Phys. **16**, 407 (1961); E. Barouch, B.M. McCoy, and M. Dresden, Phys. Rev. A **2**, 1075 (1970); E. Barouch and B.M. McCoy, Phys. Rev. A **3**, 786 (1971).
39. P. Pfeuty, Ann. Phys. (New York) **57**, 79 (1970).
40. M. Zhong and P. Tong, J. Phys. A: Math. Theor. **43**, 505302 (2010).
41. T. J. Osborne and M. A. Nielsen, Phys. Rev. A **66**, 032110 (2002).
42. J. Maziero *et al.*, Phys. Rev. A **82**, 012106 (2010).
43. O. F. Syljuåsen, Phys. Rev. A **68**, 060301(R) (2003); O. F. Syljuåsen, Phys. Lett. A **322**, 25 (2004); A. Osterloh, G. Palacios, and S. Montangero, Phys. Rev. Lett. **97**, 257201 (2006); T. R. de Oliveira et al., Phys. Rev. A **77**, 032325 (2008); B. Tomasello *et al.*, Europhys. Lett. **96**, 27002 (2011).